Journal of Manufacturing Processes 56 (2020) 1252–1262

Contents lists available at ScienceDirect

Journal of Manufacturing Processes

journal homepage: www.elsevier.com/locate/manpro

Stability boundary and optimal operating parameter identification in milling using Bayesian learning

Jaydeep Karandikar[a,*], Andrew Honeycutt[a], Tony Schmitz[a,b], Scott Smith[a]

[a] Energy and Transportation Science Division, Oak Ridge National Laboratory, Oak Ridge, TN, 37830, USA
[b] Department of Mechanical, Aerospace, and Biomedical Engineering, University of Tennessee, Knoxville, Knoxville, TN, 37996, USA

ARTICLE INFO

Keywords:
Machining
Stability
Uncertainty
Bayesian machine learning
Experimental design

ABSTRACT

This paper describes a novel Bayesian learning approach for stability boundary and optimal parameter identification in milling without the knowledge of the underlying tool dynamics or material cutting force coefficients. The paper is divided into two parts. First, a Bayesian learning method for stability lobe identification using test results is described. Each axial depth and spindle speed combination is characterized by a probability of stability which is updated using Bayes' rule when a test result (stable or unstable) is made available. A novel likelihood function is defined which incorporates knowledge of the stability behavior. Numerical results show convergence to the analytical stability lobe diagram. Second, an adaptive experimental strategy to identify optimal operating parameters that maximize material removal rate is described. Numerical evaluation shows convergence to the optimal operating point with error less than 15 % within ten tests on average. The approach is validated using experimental results. Results show that the proposed method is an efficient and robust learning method to identify the stability lobe diagram and optimal operating parameters with a limited number of tests/data points.

1. Introduction

High[1] speed machining remains an important capability for discrete part manufacturing. To select operating parameters, the stability lobe diagram, which separates the stable axial depth of cut - spindle speed combinations from unstable (or chatter) combinations, may be used [1].

The regeneration of surface waviness during material removal is the primary mechanism for chatter in machining [1–5]. With the stability lobe diagrams, the 'best' spindle speeds may be selected that enable stable machining at higher axial depths of cut. The best spindle speeds occur where the tooth passing frequency is an integer fraction of the natural frequency that corresponds to the most flexible structural mode of vibration [1]. For a given tool-material combination, calculating the stability lobe diagram requires knowledge of the tool point frequency response function and the cutting force coefficients. The frequency response is measured using a tap-test, where an instrumented hammer is used to 'tap' the tool and the corresponding response is measured using a transducer (such as an accelerometer). Each tool-holder-spindle-machine combination has a unique frequency response and needs to be measured with a tap test or calculated analytically (for example, using receptance coupling substructure analysis) [6]. The mechanistic cutting force coefficients for the tool-material combination are determined using a linear regression to the mean force values measured over a range of feed per tooth values [7]. These two input requirements can impose a significant hurdle for implementing the stability lobe diagram to maximize material removal rate in a production environment. Without knowledge of the tool point frequency response and the cutting force coefficients for the tool-material combination, machining parameters are typically determined using tool supplier and handbook recommendations, or previous experience (i.e., what worked before). If unstable behavior or chatter is observed, the parameters are 'tuned' using trial and error until stable behavior is obtained; typically, this means reducing the spindle speed and the axial depth of cut. Furthermore, although analytical and numerical models exist to predict stability, they are typically treated as deterministic and do not consider the

* Corresponding author.
E-mail address: karandikarjm@ornl.gov (J. Karandikar).

[1] This manuscript has been authored by UT-Battelle, LLC under Contract No. DE-AC05-00OR22725 with the U.S. Department of Energy. The United States Government retains and the publisher, by accepting the article for publication, acknowledges that the United States Government retains a non-exclusive, paid-up, irrevocable, world-wide license to publish or reproduce the published form of this manuscript, or allow others to do so, for United States Government purposes. The Department of Energy will provide public access to these results of federally sponsored research in accordance with the DOE Public Access Plan (http://energy.gov/downloads/doe-public-access-plan).

https://doi.org/10.1016/j.jmapro.2020.04.019
Received 25 November 2019; Received in revised form 7 February 2020; Accepted 11 March 2020
Available online 21 April 2020

Nomenclature

A	Uncertain event
B	Experimental result
N	Spindle speed
b	Axial depth of cut
i	Axial depth of cut grid point index
j	Spindle speed grid point index
p	Probability
s	Stable
u	Unstable
T	Test grid point
G	Arbitrary grid point in the domain
$+$	Stable result
$-$	Unstable result
σ_N	Standard deviation in spindle speed
σ_b	Standard deviation in axial depth of cut
K_s	Specific cutting force coefficient
MRR	Material removal rate

uncertainty in stability boundary location. This is due to inaccuracy in the measured/modeled frequency response function, cutting force coefficients, assumptions in the stability model, and factors that are not known [8–10].

To maximize material removal rates in a production environment, without knowledge of the underlying system dynamics or the tool-material cutting force coefficients, the objective of this study is to: 1) 'learn' the stability boundary using experimental results, and; 2) minimize the number of experiments required to identify the optimal stable axial depth - spindle speed combination with the highest material removal rate. Previously, Karandikar et al. used a Bayesian random walk approach to identify optimal stable parameter combinations using profit as the objective function [11]. The random walk method has two limitations. First, it is computationally expensive to generate the initial paths. Second, as the paths are filtered with each update, the updated model becomes coarse and loses accuracy. There are two main contributions to this paper. First, a novel Bayesian learning approach to determine the stability boundary from experimental results is implemented by defining a prior and likelihood function that considers the underlying physics and the nature of the stability behavior. Second, an adaptive experimental strategy to identify the optimal parameter combination with the maximum material removal rate is presented. The remainder of the paper is organized as follows. Section 2 describes the Bayesian learning approach for stability lobe identification. Section 3 presents the numerical results of the proposed approach for stability lobe identification. Section 4 presents the experimental strategy for optimal parameter identification along with numerical results. Experimental results and validation are presented in Section 5. Conclusions are presented in Section 6.

2. Bayesian learning for milling stability

Bayes' rule offers a normative method for updating probabilities when new information is made available. Let $p(A)$ be the prior probability of an uncertain event A, $p(B \mid A)$ be the likelihood of obtaining an experimental result B given event A, and $p(B)$ be the probability of experimental result B. Bayes' rule calculates the posterior probability of event A given experimental result B, denoted by $p(A \mid B)$, as shown in Eq. (1).

$$p(A|B) = \frac{p(B|A)p(A)}{p(B)} \tag{1}$$

For milling stability, each axial depth - spindle speed combination is characterized using a probability of stability. The probability can be updated using Bayes' rule, shown in Eq. (1), when experimental results are available. The prior represents the initial belief and is constructed by incorporating all available information (from analytical models, theoretical considerations, available experimental data, or expert opinions) [11]. Bayesian learning offers two main advantages. First, it considers the inherent uncertainty in the model and the experimental results by using a probability distribution. Second, the prior (or the initial belief) can be updated using limited data, as opposed to the larger datasets required by neural networks or support vector machines, for example.

2.1. Constructing the prior

As noted, the prior represents the initial belief and can incorporate all available information. In this study, it is assumed that the tool point frequency response function and the cutting force coefficients for the tool-material combination are not known. The prior probabilities are determined using the knowledge that it is more likely to get an unstable cut as the axial depth is increased at any spindle speed. To illustrate, let the axial depth of cut, b, range be 0.01 mm–20 mm and spindle speed, N, range be 10000 rpm–20000 rpm. Since machining is not possible at 0 mm, the minimum axial depth of cut is taken as 0.01 mm. The space is divided into grid points with increments of 0.1 mm in the axial depth of cut and 100 rpm in spindle speed. Each grid point has a probability of stability, s, denoted by $p(s)$, and a probability of being unstable, u, denoted by $p(u)$. As each grid point can either be stable or unstable, the sum of $p(s)$ and $p(u)$ is equal to one. Fig. 1 shows the prior probability of stability in the axial depth - spindle speed domain; the colorbar denotes the probability of stability. The probability of stability decreases linearly from one at an axial depth of cut equal to 0.01 mm to 0.05 at an axial depth of cut equal to 20 mm. The prior probability of stability is not zero at 20 mm axial depth of cut because, although unlikely, there is a possibility of observing a stable result at 20 mm. A probability of 0.05 reflects the belief that the probability of a stable cut at the maximum depth of cut is small (the value can be lower or higher based on the maximum axial depth of cut selected and user beliefs about the probability of stability at that axial depth of cut). At a 0.01 mm axial depth of cut, the probability of stability is assumed to be one as the depth of cut is very small. Since the tool point frequency response is not known, the prior probability of stability as a function of axial depth of cut is the same at all spindle speeds in the spindle speed range. Fig. 2 shows the probability of stability as a function of axial depth of cut. If the frequency response and cutting force coefficients were known, a prior probability of stability map can be generated by propagating the uncertainty in model inputs through the stability model [9,12].

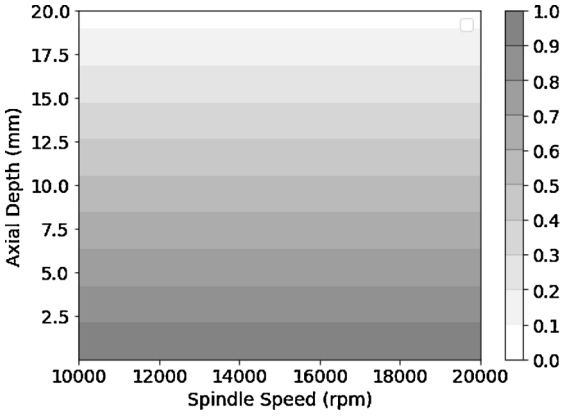

Fig. 1. Prior probability of stability.

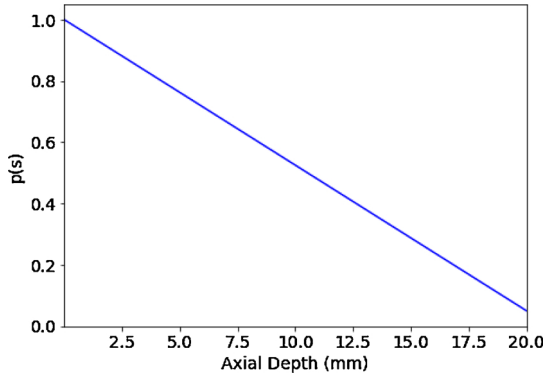

Fig. 2. Prior probability of stability as a function of axial depth of cut.

2.2. Bayesian updating at the test point using test result

Let a stable result test be denoted by '+' and an unstable result by '-'. Consider a stable result at the test point, denoted by T. The axial depth of cut and the spindle speed at the test point T are denoted by b_T, and N_T, respectively. Eq. (2) shows Bayes' rule to update the probability of stability at the test point for a stable test result at the test point. In Eq. (2), $p(s_T)$ is the prior probability of stability at T, $p(+_T \mid s_T)$ is the likelihood probability of observing a stable result at T given T is stable, and $p(+_T)$ is the probability of observing a stable result at T. The posterior probability of stability at T given a stable result at T is denoted by $p(s_T \mid +_T)$. The prior probability of stability at the test point is obtained from Fig. 2. The likelihood probability of observing a stable result at T given T is stable is one. The probability of observing a stable result at T is calculated as shown in Eq. (3) using the law of total probability. In Eq. (3), $p(u_T)$ is the prior probability of T being unstable and $p(+_T \mid u_T)$ is the likelihood probability of a stable result at T given T is unstable.

$$p(s_T|+_T) = \frac{p(+_T|s_T)p(s_T)}{p(+_T)} \tag{2}$$

$$p(+_T) = p(+_T|s_T)p(s_T) + p(+_T|u_T)p(u_T) \tag{3}$$

In Eq. (3), as stated, the likelihood probability of a stable result at T given T is stable, $p(+_T \mid s_T)$, is equal to one. The likelihood probability of a stable result at T given T is unstable, $p(+_T \mid u_T)$, is equal to zero. Substituting the probability values in Eq. (2), the posterior probability of stability at T given stable result at T is one, as shown in Eq. (4). Similarly, it can be shown that the posterior probability of stability at T given an unstable result at T, $p(s_T \mid -_T)$, is zero.

$$p(s_T|+_T) = \frac{1 \times p(s_T)}{1 \times p(s_T) + 0 \times p(u_T)} = 1 \tag{4}$$

2.3. Bayesian learning of stability in the axial depth - spindle speed domain

Bayes' rule can be used to update the probability of stability in the entire axial depth - spindle speed domain. The goal is to calculate the posterior probability of stability at each grid point given test result, stable or unstable, at T. Let G denote any arbitrary grid point in the axial depth - spindle speed domain. The axial depth of cut and the spindle speed at the grid point G are denoted by b_i, and N_j, respectively, where i and j increment along the axial depth of cut range and the spindle speed range, respectively. At the test point T, $b_i = b_T$ and $N_j = N_T$. Eqs. (5) and (6) shows Bayes' rule to update the probability of stability at any grid point G given stable result at the test point T. In Eqs. (5) and (6):

- $p(s_G \mid +_T)$ is the posterior probability of stability at a grid point G given stable test result at test point T;
- $p(s_G)$ is the prior probability of stability at G;
- $p(u_G)$ is the prior probability of G being unstable;
- $p(+_T \mid s_G)$ is the likelihood probability of a stable result at T given G is stable; and
- $p(+_T \mid u_G)$ is the likelihood probability of a stable result at T given G is unstable.

The posterior probability of G being unstable given a stable result at T, $p(u_G \mid +_T)$, can be determined by subtracting $p(s_G \mid +_T)$ from one. As stated, each grid point has a probability of stability and a probability of being unstable which sum to unity, $(p(s_G) + p(u_G) = 1)$. To calculate the posterior probability of stability at each grid point, the likelihood probabilities, $p(+_T \mid s_G)$ and $p(+_T \mid u_G)$ need to be determined. Note that the denominator, $p(+_T)$, will vary with each grid point; see Eq. (6). If $p(+_T \mid s_G)$ is equal to $p(+_T \mid u_G)$, the posterior probability of stability at G, $p(s_G \mid +_T)$, is equal to the prior probability of stability, $p(s_G)$, since $p(s_G) + p(u_G) = 1$. This is shown in Eq. (7).

$$p(s_G|+_T) = \frac{p(+_T|s_G)p(s_G)}{p(+_T)} \tag{5}$$

$$p(+_T) = p(+_T|s_G)p(s_G) + p(+_T|u_G)p(u_G) \tag{6}$$

$$p(s_G +_T) = \frac{p(+_T|s_G)p(s_G)}{p(+_T|s_G)(p(s_G) + p(u_G))} = \frac{p(+_T|s_G)p(s_G)}{p(+_T s_G) \times 1} = p(s_G) \tag{7}$$

To determine the likelihood probabilities, the following assessments can be made from knowledge of the stability behavior. First, the influence of the test result will reduce as the distance from the test point increases. In Bayesian terms, this means that the posterior probability of stability will be equal to the prior probability of stability (or change in the prior probability of stability will reduce to zero) after a certain distance from the test point. However, due to the nature of the machining stability, the influence of the test point is not symmetric along the axial depth of cut and the spindle speed range. At the test spindle speed, a stable result implies that all axial depths of cut below the test axial depth of cut are also stable. Therefore, a stable result will have a larger influence along spindle speed at axial depths of cut smaller than the test axial depth of cut. Furthermore, the smaller the axial depth of cut, the larger the influence of the stable result since the width of the stability lobe along the spindle speed increases at lower axial depths of cut. A stable result at the test point does not provide any information for stability at higher axial depths of cut; therefore, the influence of the test result reduces at higher axial depth of cut values. At a selected axial depth of cut, the influence of the test result is treated as symmetric about the test spindle speed. This is illustrated in Fig. 3. For an unstable result, the opposite is true. An unstable result implies all axial depths of cut higher than the test axial depth at the test spindle speed are unstable. Therefore, the influence of an unstable result along spindle

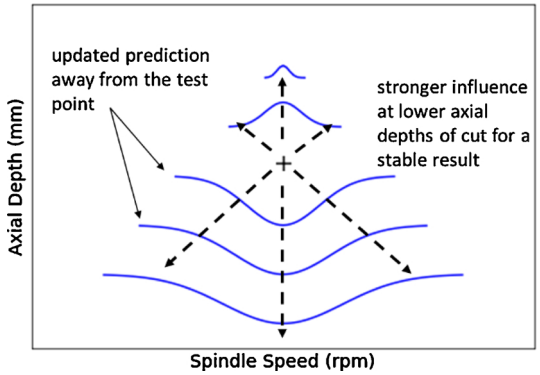

Fig. 3. Influence of a stable result; a stable result implies all axial depths of cut below the test axial depth of cut are also stable resulting in a larger influence.

speed increases with axial depth of cut.

For demonstration purposes, consider a stable result at test point T at $\{b_T = 10$ mm, $N_T = 15{,}000$ rpm$\}$. The posterior probability of stability at T is equal to 1 as shown in Eq. (4). The objective is to calculate the posterior probability of stability at all grid points in the domain given the stable test result at $T = \{10$ mm, 15,000 rpm$\}$. Recall that in order to calculate the posterior probability of stability at any grid point, G, given stable test result at T, the likelihood probabilities $p(+_T \mid s_G)$ and $p(+_T \mid u_G)$ need to be determined. Consider six candidate grid points as shown in Fig. 4, denoted by J, K, L, M, N, and O. Table 1 lists the axial depth of cut, spindle speed, and the prior probability of stability at each grid point (from Figs. 1 and 2). The following assessments can be made for $p(+_T \mid s_G)$ for each point:

- $p(+_T \mid s_T)$ is one;
- a stable test result at T implies a stable test result at L (lower axial depth of cut at the same spindle speed); for simplicity, $p(+_T \mid s_L)$ can be replaced by $p(+_L \mid s_L)$ which is one;
- $p(+_T \mid s_N)$ is also equal to 1, since if a grid point is known to be stable, all axial depths of cut smaller than the grid point axial depth of cut are also stable;
- the likelihood probability of a stable result at T given grid point is stable reduces from one along the spindle speed - $p(+_T \mid s_T) > p(+_T \mid s_J) > p(+_T \mid s_K)$;
- $p(+_L \mid s_M) > p(+_T \mid s_J)$ since the width of the stability lobe increases at smaller axial depth of cut.

The following assessments can be made for $p(+_T \mid u_G)$:

- $p(+_T \mid u_T)$ and $p(+_L \mid u_L)$ is zero;
- at axial depths of cut smaller than b_T, the likelihood probability of a stable result at T given the grid point is unstable increases from zero along the spindle speed - $p(+_T \mid u_T) < p(+_T \mid u_J) < p(+_T \mid u_K)$;
- at N_T, the likelihood probability of a stable result at T given grid point is unstable increases with axial depth of cut - $p(+_T \mid u_T) < p(+_T \mid u_N)$.

As the distance from T increases, the influence of the test result reduces such that $p(+_T \mid s_G)$ and $p(+_T \mid u_G)$ are equal giving $p(s_G \mid +_T)$ is equal to $p(s_G)$ as shown in Eq. (7). The influence of the test result along spindle speed at b_T was defined by a Gaussian standard deviation, denoted by σ_{NbT}. $p(+_T \mid s_G)$ is calculated using Gaussian probability densities with the test spindle speed as the mean and σ_{NbT} as the standard deviation. As noted, $p(+_T \mid s_G)$ decreases from one at N_T along the spindle speed. The minimum value is 0.5 since the uncertainty is maximum as the distance from the test point increases. Since $p(+_T \mid u_G)$ increases from zero along spindle speed, it is calculated by subtracting $p(+_T \mid s_G)$ from one. $p(+_T \mid s_G)$ and $p(+_T \mid u_G)$ as a function of spindle speed at the test axial depth of cut, b_T, is given by Eqs. (8) and (9), respectively.

$$p(+_T \mid s_G)_{N_j, b_T} = 0.5 + \frac{e^{-0.5\left(\frac{(N_j - N_t)}{\sigma_{N b_T}}\right)^2}}{2} \tag{8}$$

$$p(+_T \mid u_G)_{N_j, b_T} = 1 - p(+_T \mid s_G)_{N_j, b_T} \tag{9}$$

$p(+_T \mid s_G)$ and $p(+_T \mid u_G)$ converge to 0.5 at $N_j = N_T \, 3\sigma_{NbT}$; this restricts the influence of the test result to $3\sigma_{NbT}$. As shown in Eq. (7), if $p(+_T \mid s_G)$ and $p(+_T \mid u_G)$ are equal, the posterior probability at the grid point is equal to the prior probability. Fig. 5 shows the likelihood probabilities as a function of spindle speed at $b_T = 10$ mm with $\sigma_{NbT} = 300$ rpm. Recall that the test point T is at $\{b_T = 10$ mm, $N_T = 15{,}000$ rpm$\}$. From Fig. 5, the likelihood probabilities, $\{p(+_T \mid s_G), (+_T \mid u_G)\}$, for points T, J, and K, are {1.0, 0.0}, (0.62, 0.38}, and {0.5, 0.5}, respectively. The likelihood probabilities are equal for point K since it is outside the N_T $3\sigma_{NbT}$ influence of the test point at 14,000 rpm. The posterior probability at each grid point can be calculated using Eqs. (5) and (6) by substituting $p(+_T \mid s_G)$ and $p(+_T \mid u_G)$ from Fig. 5 and the prior probability of stability, $p(s_G)$, from Fig. 2. Recall that $p(u_G) = 1 - p(s_G)$. Fig. 6 shows the posterior probability of stability as a function of spindle speed at $b_T = 10$ mm given a stable result at {10 mm, 15,000 rpm}. From Fig. 6, the posterior probability at points T, J, and K is 1.0, 0.64, and 0.52, respectively. From Figs. 1 and 2, the prior probability of stability at 10 mm at all spindle speeds was 0.52. As shown in Eqs. (2) and (4), the posterior probability of stability at T given stable result at T is one. At J, the posterior probability of stability increases to 0.64 from 0.52. At K, there is no change in the probability of stability since the likelihood probabilities are equal. As noted, the posterior probability converges to the prior probability at 3 σ_{NbT} (900 rpm) distance from the test speed.

Updating the probabilities at axial depth of cut values lower than the test axial depth of cut is straightforward. As noted, from the knowledge of the stability lobe diagram, a stable result at b_T implies that all axial depth of cut values smaller than b_T at N_T are also stable. Therefore, for simplicity, a stable result can be added to all axial depths smaller than b_T. The likelihood probability values along spindle speed at each axial depth of cut, $b_i < b_T$, was determined using the procedure described to calculate the probabilities at b_T (Eqs. (8) and (9)). However, note that the influence of the stable result will be higher at lower axial depths of cut due to the nature of the stability lobe diagrams where the width of the lobe increases at lower axial depths of cut. This is enforced by increasing the value of σ_N at lower axial depths of cut for a stable result. In Eqs. (8) and (9), σ_{NbT} is not constant, but increases at $b_i < b_T$. The relationship of σ_N with the axial depth of cut is described later in the section and shown in Fig. 11. Fig. 7 shows the likelihood probabilities (left) and the posterior and prior probability of stability (right) at 10 mm and 6 mm axial depth of cut with $\sigma_N = 300$ rpm at 10 mm and $\sigma_N = 500$ rpm at 6 mm. From Fig. 7, the likelihood probabilities for points L, and M, are {1.0, 0.0}, and {0.8, 0.2}, respectively. As stated, the likelihood probability, $p(+ \mid s)$, is higher at M than J since M is at a smaller axial depth of cut. The posterior probability of stability at L, and M is 1.0, and 0.9, respectively. Note that the prior probability of stability at 6 mm is 0.71 (see Fig. 2). At both axial depths of cut, the posterior probability is equal to the prior probability at $N_T \pm 3 \times \sigma_N$.

As noted, at the test spindle speed, at the axial depth of cut values higher than b_T, $p(+_T \mid s_G)$ is equal to one and $p(+_T \mid u_G)$ increases from zero. The influence of the stable test result at axial depths of cut higher than the test axial depth is defined using a standard deviation along the axial depth, denoted by σ_b. $p(+_T \mid u_G)$ is calculated using non-normalized Gaussian probability densities with $(b_T + 3\sigma_b)$ as the mean and σ_b as the standard deviation. Recall that $p(+_T \mid u_G)$ is zero at b_i b_T. Like spindle speed, the objective is to restrict the influence of a stable result to $b_T + 3\sigma_b$. $p(+_T \mid u_G)$ is kept equal to one at b_i $b_T + 3\sigma_b$; this ensures $p(+_T \mid s_G)$ and $p(+_T \mid u_G)$ are equal to one at b_i $b_T + 3\sigma_b$. $p(+_T \mid u_G)$ as a function of axial depth at the test spindle speed is given by Eq. (10):

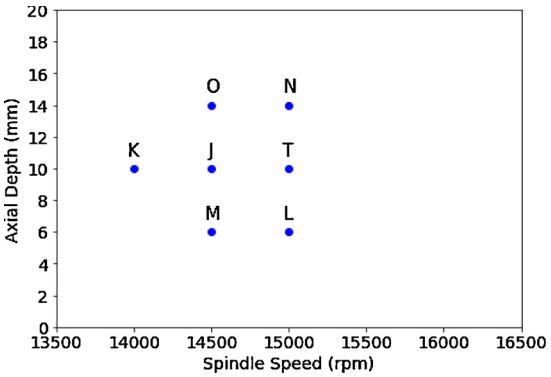

Fig. 4. Candidate grid points for calculating the posterior probability of stability given stable test result at T at {10 mm, 15,000 rpm}.

Table 1
Axial depth of cut, spindle speed, and prior probability of stability at each grid points.

	Axial depth of cut (mm)	Spindle speed (rpm)	$p(s)$
T	10	15,000	0.52
J	10	14,500	0.52
K	10	14,000	0.52
L	6	15,000	0.70
M	6	14,500	0.70
N	14	15,000	0.33
O	14	14,500	0.33

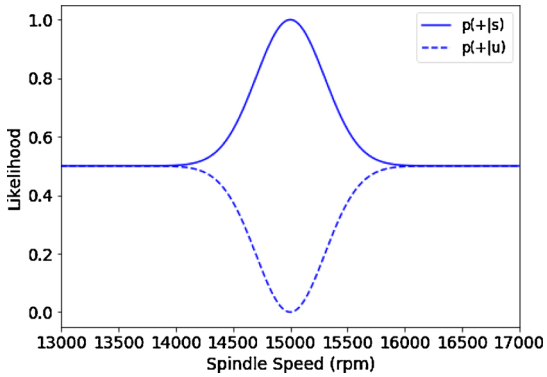

Fig. 5. The likelihood of stable result at T at $\{b_T = 10$ mm, $N_T = 15{,}000$ rpm$\}$ given grid point is stable (solid line) and given the grid point is unstable (dashed line) as a function of spindle speed at 10 mm depth of cut.

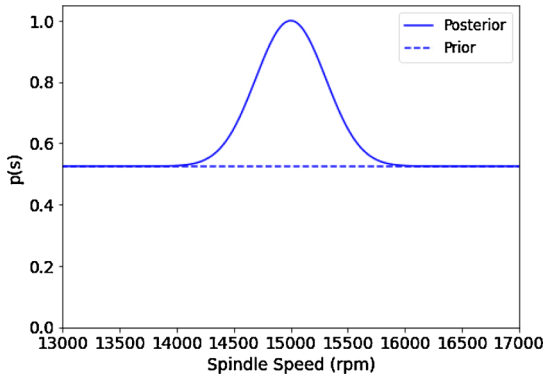

Fig. 6. Posterior and prior probability of stability as a function of spindle speed at 10 mm depth of cut given stable result at T at $\{b_T = 10$ mm, $N_T = 15{,}000$ rpm$\}$.

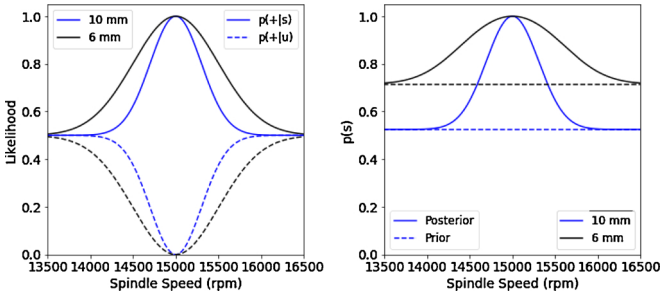

Fig. 7. Likelihood probabilities (left) and posterior and prior probability of stability (right) at 10 mm and 6 mm axial depth of cut; note that a test result was added at all axial depths lower than the test axial depth $b_T = 10$ mm.

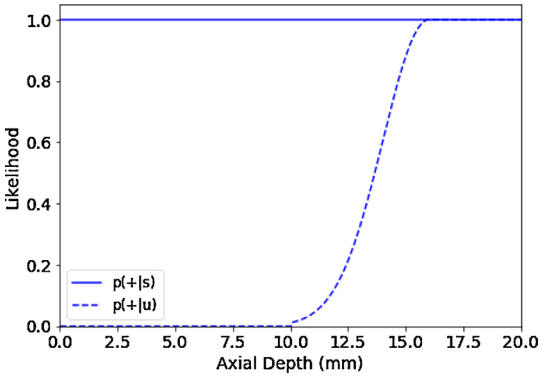

Fig. 8. The likelihood of a stable result at T at $\{b_T = 10$ mm, $N_T = 15{,}000$ rpm$\}$ given grid point is stable (solid line) or unstable (dashed line) as a function of axial depth of cut at 15,000 rpm.

$$p(+_T \mid u_G)_{N_T,\, b_i} = \begin{cases} 0, & b_i \le b_T \\ e^{-0.5\left(\frac{(b_i-(b_t+3\sigma_b)}{\sigma_b}\right)^2}, & b_T < b_i \le b_T + 3\sigma_b \\ 1, & b_i > b_T + 3\sigma_b \end{cases} \tag{10}$$

As a result, the posterior probability of stability equals the prior probability of stability at b_i $b_T + 3\sigma_b$ at the test spindle speed. This restricts the influence of a stable result at the higher axial depth of cut values to $b_T + 3\sigma_b$. Fig. 8 shows the likelihood probabilities as a function of axial depth at the test spindle speed of 15,000 rpm with $\sigma_b = 2$ mm. Recall that at axial depth lower than the test axial depth, stable results were added from the knowledge of the stability lobe diagram giving the likelihood probability $p(+_T \mid s_G)$ equal to one at all axial depths of cut. From Fig. 8, the likelihood probabilities, $p(+_T \mid s_N)$, and $p(+_T \mid u_N)$, for point N are 1.0 and 0.6, respectively. Fig. 9 shows the posterior probability of stability as a function of axial depth of cut at the test spindle speed calculated using Eqs. (5) and (6). The posterior probability of stability at N is 0.45. As seen from Fig. 9, the posterior probability of stability converges to the prior probability of stability at $b_T + 3\sigma_b$ (16 mm); this is enforced by the equal likelihood probabilities as shown in Fig. 8. From Fig. 2, the prior probability of stability decreases from 1 at 0.01 mm to 0.05 at 20 mm.

The likelihood probabilities, $p(+_T \mid s_G)$ and $p(+_T \mid u_G)$, along the spindle speed at axial depth of cut values higher than the test axial depth, were calculated by reducing the σ_{NbT} value linearly to zero at $b_T + 3\sigma_b$. This reduces the influence of the stable result along spindle speed at $b_i > b_T$ as shown in Fig. 3. At each depth of cut, note that the values are scaled between one to 0.5 for $p(+_T \mid s_G)$, and between 0.5 to the likelihood value given by Eq. (10) for $p(+_T \mid u_G)$. $p(+_T \mid s_G)$ and $p(+_T \mid u_G)$ for $b_i > b_T$ are given by Eqs. (11) and (12):

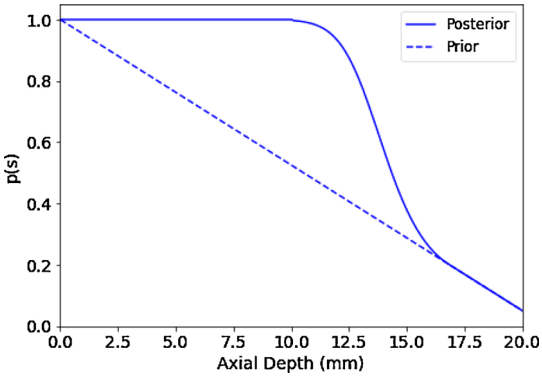

Fig. 9. Posterior and prior probability of stability as a function of axial depth of cut at 15,000 rpm given stable result at T at $\{b_T = 10$ mm, $N_T = 15{,}000$ rpm$\}$.

$$p(+_T \mid s_G)_{N_j, b_i > b_T} = 0.5 + \frac{e^{-0.5\left(\frac{(N_j - N_t)}{\sigma_{N b_i}}\right)^2}}{2} \quad (11)$$

$$p(+_T \mid u_G)_{N_j, b_i > b_T} = 0.5 + \frac{e^{-0.5\left(\frac{(N_j - N_t)}{\sigma_{N b_i}}\right)^2}}{\left(\frac{1}{p(+_T \mid u_G)_{N_T, b_i}} - 0.5\right)} \quad (12)$$

Fig. 10 shows the likelihood probabilities and posterior and the prior probability of stability at 10 mm and 14 mm. From Fig. 10, the likelihood probabilities for points *N* and *O* are {1.0, 0.6} and {0.5, 0.5}, respectively. The posterior probabilities of stability at *N* and *O* are 0.45 and 0.33, respectively. Note that the prior probability at 14 mm is 0.33 (see Fig. 2). As shown in Fig. 10, the posterior probability converges to the prior probability at a faster rate at 14 mm than at 10 mm since σ_N = 100 rpm at 14 mm σ_N and =300 rpm at 10 mm. Table 2 shows $p(+_T \mid s_G)$ and $p(+_T \mid u_G)$ and the posterior probability, $p(s_G \mid +_T)$, for grid points *T, J, K, L, M, N,* and *O*.

As noted, σ_N value reduces linearly from σ_{NbT} at b_T to zero at $b_T + 3\sigma_b$. At axial depths of cut lower than b_T, σ_N increases at the same rate. Fig. 11 shows σ_N as a function of axial depth of cut; grid lines are provided for clarity. As noted, σ_{NbT} =300 rpm at b_T = 10 mm and zero at $b_T + 3\sigma_b$ = 16 mm. The value of σ_N increases linearly with the same slope at lower axial depth of cut. Eq. (13) describes the relationship of σ_N as a function of the axial depth of cut for a stable cut.

$$\sigma_N = \begin{cases} -\frac{\sigma_{N_{bT}}}{3\sigma_b} b_i + \frac{\sigma_{N_{bT}}(b_T + 3\sigma_b)}{3\sigma_b} & b_i \le b_T + 3\sigma_b \\ 0 & b_i > b_T + 3\sigma_b \end{cases} \quad (13)$$

The posterior probability of stability at each grid point is calculated from Eqs. (5) and (6) using the prior and the likelihood probabilities. Fig. 12shows the posterior probability of stability in the defined axial depth - spindle speed domain given stable result at T = {10 mm, 15,000 rpm}; the filled 'o' denotes a stable result and the colorbar gives the probability of stability. For an unstable cut, the likelihood probability values are the opposite of a stable result. An unstable cut implies that all axial depth of cut higher than the test axial depth of cut are also unstable. Therefore, at the test spindle speed, an unstable result can be added at each axial depth of cut higher than the test axial depth of cut. At the test axial depth of cut, $p(-_T \mid s_G)$ increases from zero to 0.5 and $p(-_T \mid u_G)$ reduces from one to 0.5 along the spindle speed. At axial depth of cut values lower than the test axial depth of cut, $p(-_T \mid u_G)$ is equal to one and $p(-_T \mid s_G)$ increases from zero at b_T to one at b_T - $3\sigma_b$. σ_N increases linearly at $b_i > b_T$ with the same slope. Eqs. (8)–(13) would be modified for an unstable result and are not shown here for brevity. Fig. 13 shows the updated probability of stability given an unstable result at {10 mm, 15,000 rpm}; the 'x' denotes the unstable result.

As noted, a Gaussian density function was used to calculate the likelihood probabilities. An alternative function would be a triangular distribution where the likelihood probabilities decrease linearly from 1 to 0.5. The choice of σ_N and σ_b determine the influence of test point and the posterior probabilities, which in turn, influences the width of the stability lobe after each update as shown in Fig. 12. For the updating procedure, σ_{NbT} and σ_b were selected as 300 rpm (3 % of the spindle speed range) and 2 mm (10 % of the axial depth of cut range), respectively.

3. Numerical results for stability lobe identification

As described in Section 2, Bayesian learning updates probability of stability at all grid points in the axial depth - spindle speed domain given a test result. The procedure can be extended to learn with multiple test results where the posterior probabilities of stability after the first update become the prior probabilities of stability for the second update, and so on. After the probabilities are updated using all test results, a stability lobe prediction from the Bayes' learning approach can be made at axial depths where the probability of stability is equal to 0.5. Numerical results for stability lobe identification using the Bayesian learning approach are presented in this section by comparing the Bayes' learning prediction with a known stability boundary.

Fig. 14 shows a 'true' stability lobe diagram as a solid line (referred to as Model 1) overlaid on the prior probability of stability map. The objective is to compare the stability prediction given by the Bayesian learning approach described in Section 2 with the known stability limit using numerical test results generated from the known stability diagram. The procedure to generate the numerical test results is as follows. A grid-based approach was selected with numerical stability tests at every 4 mm axial depth of cut and 500 rpm spindle speed giving a 5 × 21 test-grid (numerical tests are not done at 0.01 mm since the prior probability of stability is one). The test result, stable or unstable, was determined by comparing the test axial depth of cut with the 'true' axial depth of cut from the stability diagram shown in Fig. 14. At the test spindle speed, if the test axial depth is less than or equal to the 'true' axial depth from the known stability diagram, the result is stable; otherwise, it is unstable. Numerical tests proceed with increasing axial depths of cut until an unstable result is observed, after which, testing is terminated at that test spindle speed. This is because it is known from the stability behavior that subsequent tests at higher axial depths of cut will also be unstable at the same spindle speed. The test points move to the next spindle speed and the process is repeated at every spindle speed in the test grid. The test results were then used to update the probability of stability using the Bayes' learning procedure described in Section 2. For the updating, σ_{NbT} was 300 rpm and σ_b was 2 mm. As explained in Section 2, σ_N was not constant, but increased linearly to σ_N at b_T from zero at $b_T + 3 \times \sigma_b$ or b_T - $3 \times \sigma_b$ depending on whether the result was stable or unstable, respectively. Recall that this is because the influence of a stable result is different than an unstable result. If the result is stable, σ_N continues to increase linearly at lower axial depths of cut (see Fig. 11). If the result is unstable, σ_N increases linearly at higher axial depth of cut values. Fig. 15 shows the results. The left-hand side figure shows the posterior probability of stability given numerical test results; stable results are denoted by filled 'o' symbols and unstable results are denoted by 'x' symbols. The right-hand side figure shows the shows the predicted stability boundary corresponding to a probability of stability equal to 0.5. The 'true' underlying stability lobe diagram is also shown for reference. As seen from Fig. 16, the predicted boundary from the Bayes' learning approach shows good agreement with the true stability diagram with an average percentage error of 22 % after 42 tests. The second lobe at 11,650 rpm is not predicted by the Bayes' learning method since the test grid does not capture a stable result in the lobe; a finer grid with smaller spacing in spindle speed will capture the lobe at 11,650 rpm. To illustrate, a finer grid with tests at every 2 mm axial depth of cut and 250 rpm spindle speed giving a 11 × 41 grid results in average percentage error of 11.2 % after 163 tests; Fig. 16 shows the results.

To evaluate the robustness of the Bayes' learning approach, three

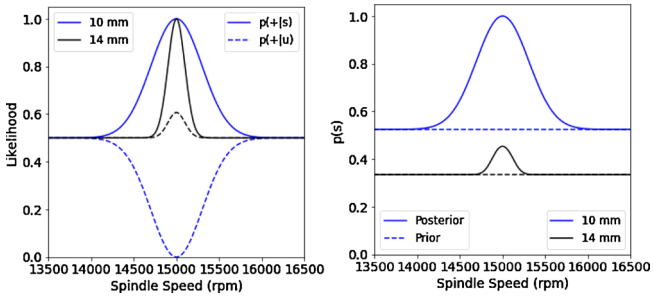

Fig. 10. Likelihood probabilities (left) and posterior and prior probability of stability (right) at 10 mm and 14 mm axial depth of cut given stable result at T at {b_T = 10 mm, N_T = 15,000 rpm}.

Table 2
Axial depth of cut, spindle speed, and prior probability of stability at each grid point.

	Axial depth of cut (mm)	Spindle speed (rpm)	$p(s)$	$p(u)$	$p(+\|s)$	$p(+\|u)$	$p(s\|+)$
T	10	15,000	0.52	0.48	1.0	0.0	1.0
J	10	14,500	0.52	0.48	0.62	0.38	0.64
K	10	14,000	0.52	0.48	0.50	0.50	0.52
L	6	15,000	0.71	0.29	1.0	0.0	1.0
M	6	14,500	0.71	0.29	0.80	0.20	0.90
N	14	15,000	0.33	0.67	1.0	0.60	0.45
O	14	14,500	0.33	0.67	0.50	0.50	0.33

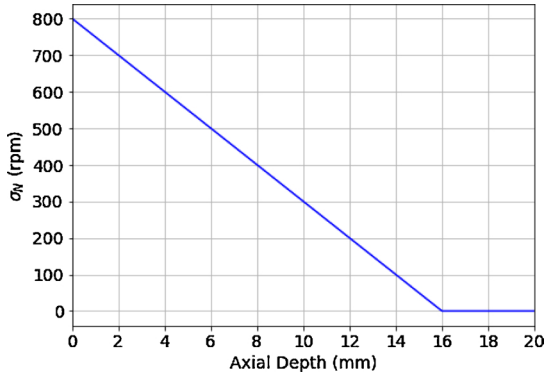

Fig. 11. σ_N as a function of axial depth of cut.

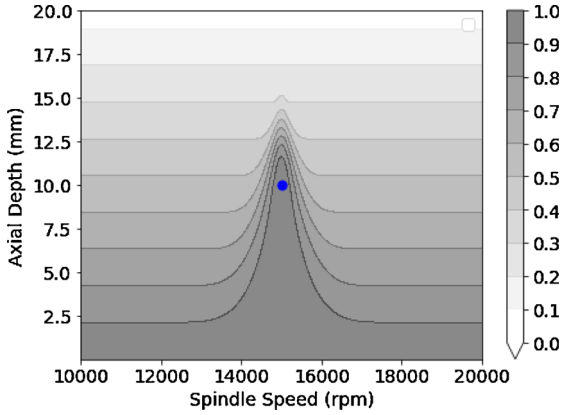

Fig. 12. Posterior probability of stability given stable result at {10 mm, 15,000 rpm}, denoted by the filled 'o'.

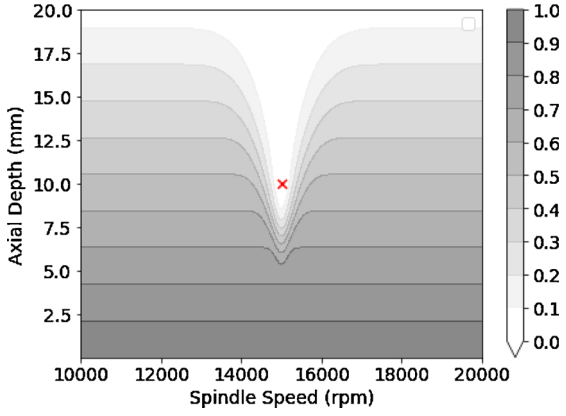

Fig. 13. Posterior probability of stability given unstable result at {10 mm, 15,000 rpm}, denoted by the 'x'.

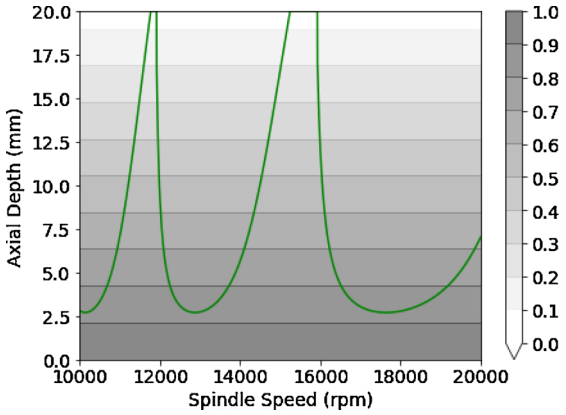

Fig. 14. Prior probability of stability with the true stability lobe diagram used for numerical evaluation.

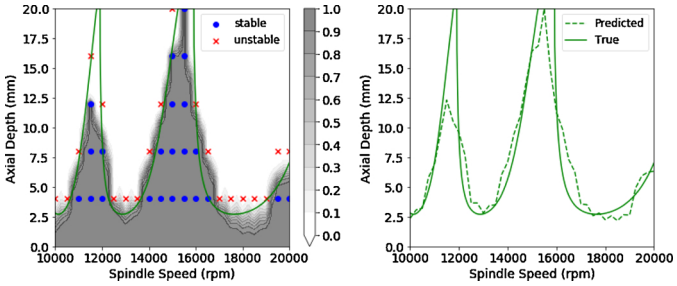

Fig. 15. Posterior probability of stability given numerical test results (left) and comparison of the Bayes' learning predicted and true stability lobe diagram (right) with a 10 × 11 grid.

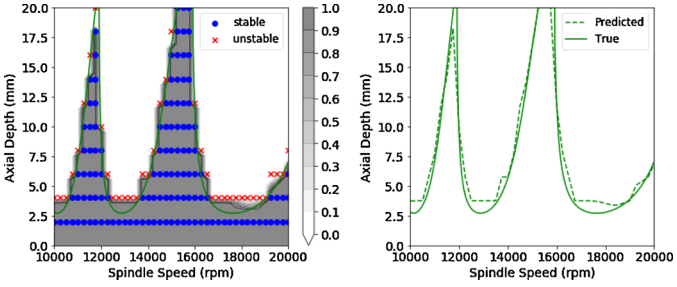

Fig. 16. Comparison of the Bayes' learning predicted and true stability lobe diagram.

additional models were tested with different axial depth - spindle speed ranges. The σ_b and σ_{NbT} were parametrized as 10 % and 3 % of the axial depth of cut and spindle speed range, respectively. A 5 × 21 test-grid was selected for each model for numerical experiments. Fig. 17 displays the results; the left-hand side figure shows the posterior probability of stability and the right-hand side figure shows the comparison of the Bayes' learning predicted model with the true model. Results show good agreement with Bayes' stability boundary prediction and the true boundary. The average percentage error between the 'true' and predicted stability boundary is 19.2 %, 12.0 %, and 17.9 %, for Model 2 (top row), Model 3 (middle row), and Model 4 (bottom row), respectively. As shown, a finer grid with smaller spacing in axial depth of cut and spindle speed will lead to a better agreement with the true boundary as all the lobes will be captured by a stable result. A 10 × 41 grid for Model 2, Model 3, and Model 4 gives an average percentage error equal to 18.5 %, 5.6 %, and 5.9 %, respectively. The results are not shown for brevity.

The Bayes' learning method offers several advantages over machine learning methods such as neural networks or support vector machines

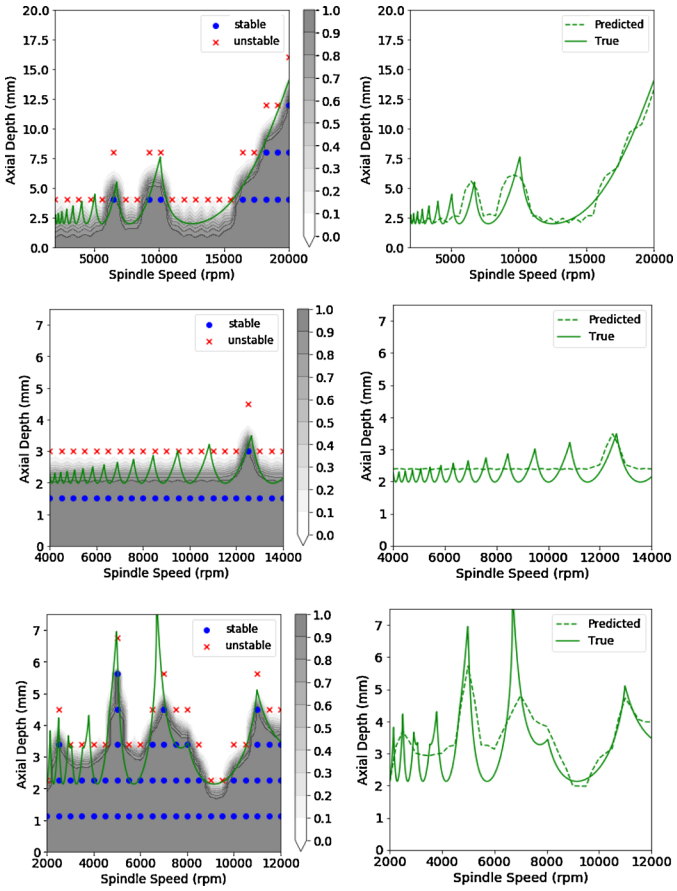

Fig. 17. Comparison of the Bayes' learning stability boundary prediction with the true boundary; results show good agreement.

for stability lobe identification. First, and most important, updating can be done with small data. As shown in Figs. 10 and 11, even a single test result updates the probability of stability. This enables continuous learning in a production industrial environment when large number of data points may not be available. Second, all available information about the stability diagram can be encoded in the prior. Third, process knowledge can be incorporated in the framework to guide the learning model.

4. Experimental strategy for optimal parameter identification

As noted, calculating the stability boundary using the analytical model requires knowledge of the tool point frequency response function and cutting force coefficients for the tool-material combination. This can impose a significant hurdle in identifying the optimal machining parameters in an industrial environment. Without this information and the corresponding stability map, selection of machining parameters is typically done using tool supplier or handbook recommendations. This section presents an adaptive experimental strategy to minimize the number of experiments required to identify the optimal stable machining parameters with the highest material removal rate (*MRR*).

As shown in Section 2, each test result updates the probability of stability in the axial depth - spindle speed domain. The objective is to find the axial depth - spindle speed combination with the highest *MRR* which is stable with certainty (or probability of stability equal to one). Bayes' learning combined with decision analysis enables a value to be placed on the information from an experiment prior to performing it; this is called the value of information [13,14]. To find the optimal operating point with the highest *MRR*, value of information is defined as the expected percentage improvement in *MRR* after testing. To illustrate the methodology, consider Model 1 shown in Fig. 14. Before any experiments are performed, the optimal operating parameters are {0.01 mm, 20,000 rpm} from the prior. This is because the prior probability of stability is one at 0.01 mm at all spindle speeds and the maximum *MRR* is at the maximum spindle speed equal to 20,000 rpm. For a given tool, feed per tooth, and radial depth of cut, the *MRR* at {0.01 mm, 20,000 rpm} will be proportional to 0.01 mm × 20,000 rpm = 200 mm-rpm. Consider grid-point point P = {0.5 mm, 20,000 rpm}. The prior probability of stability at point P is 0.97. The procedure to calculate the expected percentage improvement in *MRR* after testing at P is as follows. If P is stable, the posterior probability of stability at P and all axial depths of cut below 0.5 mm are equal to 1. Although the posterior probability of stability of points in neighboring spindle speeds increases, it will not be equal to one. Thus, P becomes the new optimal point since it has the maximum *MRR* from all points known to be stable with certainty. The *MRR* at P is proportional to 0.5 mm × 20,000 rpm = 10,000 mm-rpm. The percentage improvement in *MRR* from the last optimal point, {0.01 mm, 20,000 rpm} with material removal rate proportional to 200 mm-rpm, will be 4900 % (calculated as). If P is unstable, the optimal point remains at {0.01 mm, 20,000 rpm}. This is because an unstable result does not provide any information on additional stable points. Therefore, the improvement in *MRR* if P is unstable is 0 %. The expected percentage improvement in *MRR* at P is calculated as:

$$\%\ \text{improvement in } MRR = 0.97 \times 4900 + 0.03 \times 0 = 4753.0$$

In equation form, the expected percentage improvement in MRR is given by:

$$E[I(\%MRR)] = p(s_g) \times \frac{(MRR_g - MRR_{prior}) \times 100}{MRR_{prior}} + p(u_g) \times 0 \tag{14}$$

In Eq. (14), MRR_{prior} is the *MRR* for the last known optimal point, and MRR_g is the *MRR* at the grid point. The expected percentage improvement in *MRR* is calculated at all grid points in the domain; the optimal test point is where the value is maximum. Fig. 18 shows the expected percentage improvement in *MRR* at all axial depth - spindle speed grid points; the colorbar shows the expected percentage improvement in *MRR*. The optimal test parameter is {10.1 mm, 20,000 rpm} with a prior probability of stability equal to 0.50 and expected percentage improvement in *MRR* equal to 56000 %; the point is identified by a solid (half) circle in Fig. 18. From Model 1 shown in Fig. 14, {10.1 mm, 20,000 rpm} is unstable. Fig. 19 shows the updated probability of stability given an unstable result at {10.1 mm, 20,000 rpm}.

As noted, the posterior probabilities of stability after the first update become the prior probabilities of stability for the second update. The expected percentage improvement in *MRR* was calculated using the

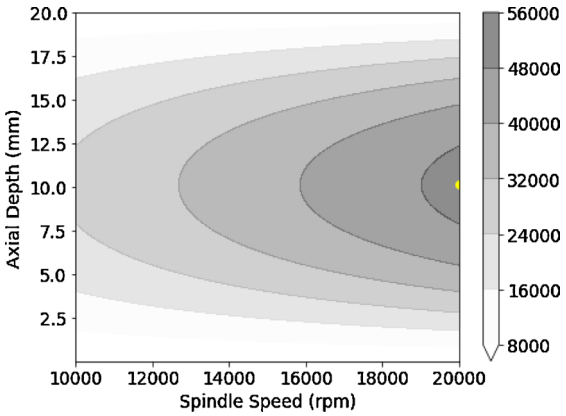

Fig. 18. Expected percentage improvement in *MRR*; the solid (half) circle identifies the optimal test parameter at {10.1 mm, 20,000 rpm} with a maximum expected percentage improvement equal to 56000 %.

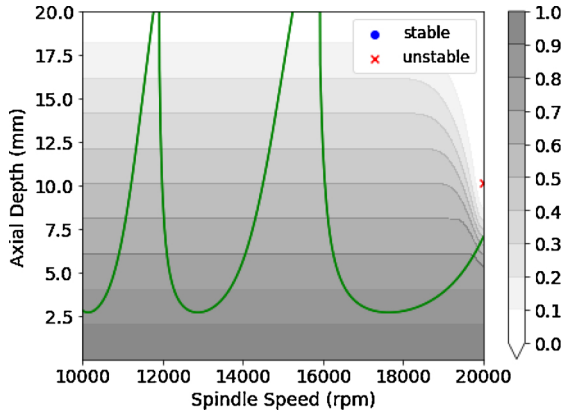

Fig. 19. Updated posterior probability given unstable result at {10.1 mm, 20,000 rpm}.

posterior probabilities after the first test. Fig. 20 shows the expected percentage improvement in *MRR* (left) for the second test; the optimal test point was {9.61 mm, 19,000 rpm}. As seen from Fig. 19, the posterior probability of stability at axial depth greater than 10.1 mm is zero due to the unstable test result at {10.1 mm, 20,000 rpm}. The posterior probability of stability at axial depth of cut below 10.1 mm also reduces due to the unstable result. As a result, the second optimal test shifts left to a smaller spindle speed at a smaller axial depth of cut. Fig. 20 (right) shows the posterior probabilities after the second update. As shown in Fig. 20, the maximum expected improvement in *MRR* reduces to 48000 % for the second test as compared to 56000 % for the first test. The procedure was repeated until the maximum expected improvement in *MRR* was less than 5 %. Note that once a stable result was observed at a test point, the test point becomes the new optimal point and subsequent calculation are based on the expected improvement in *MRR* from the new optimal point.

Fig. 21 shows the results. The test points are marked based on the order of testing. The experiments terminate after Test 14 when the maximum expected percentage improvement in *MRR* is less than 5 %. Fig. 22 shows the maximum expected percentage improvement in *MRR* for each test. The reduction in value at Test 10 occurs as the first stable result is observed at Test 9 at {9.5 mm, 15,300 rpm}. Therefore, the Test 9 parameters become the new optimal and the expected percentage improvement in *MRR* for Test 10 is calculated from the *MRR* at Test 9. Similarly, the Test 10 parameters become the new optimal since it is also stable and the expected percentage improvement for Test 11 is based on *MRR* at the Test 10 parameters. Each stable result becomes the new optimal for subsequent calculations. After 14 tests, the optimal parameter identified by the experimental procedure is {18.51 mm, 15,300 rpm}. The true optimal point is {20 mm, 15,930 rpm}. The error between the identified optimal *MRR* and the true optimal *MRR* is 11.2 %.

To evaluate the robustness of the proposed experimental search method, the experimental procedure was repeated on Model 2, Model 3, and Model 4. Recall that the search terminates when the maximum expected percentage improvement in *MRR* is less than 5 %. Fig. 23 shows the results. The error between the optimal MRR from the search and the 'true' optimal *MRR* from the known stability boundary was 7.8 %, 16.6 %, and 1.8 %, for Model 2, Model 3, and Model 4, respectively within 3–14 tests. The proposed methodology is a greedy search and may fail to converge to the global optimum at a lower speed if a local optimal is found at a higher speed. This can arise due to process damping at lower speeds resulting in higher stable axial depths of cut. Two updates can be made to the search strategy to find the global optima at lower spindle speeds. First, a smaller stopping criterion for expected percentage improvement in *MRR* may be selected such as 1 %. Second, the spindle speed range may be divided into two or more equal grids and the search may be performed independently in each grid. This will ensure that the algorithm finds multiple stable parameters across the range of spindle speeds. This approach is especially beneficial in cases where tool wear is a limiting factor.

5. Experimental validation

The Bayes' learning procedure for stability lobe and optimal parameter identification was validated using experiments. Milling tests were performed using a 12.7 mm diameter, four flute helical solid carbide endmill to machine a 6061-T6 aluminum workpiece. Fig. 24 shows the experimental setup. The tool point frequency response function (FRF) was measured using a tap test and the result is presented in Fig. 24 for the feed (X) and Y directions. The natural frequency for the tool was 2000 Hz. The axial depth of cut range and spindle speed range were selected as 0.01 mm–4 mm and 6600 rpm–10600 rpm, respectively. Stability tests were performed at each 1 mm axial depth of cut increment and 800 rpm spindle speed increments giving a 4 6 test grid. Tests were not performed at 0.01 mm. All milling operations were down milling with a 5 mm radial depth of cut and a feed per tooth of 0.1 mm. For each test, the audio signal was recorded. Stability was determined by converting the audio signal into the frequency domain using the Fast Fourier Transform (FFT) and by calculating the ratio of the chatter frequency amplitude to the fundamental tooth passing frequency amplitude, referred to as the stability ratio. If the stability ratio was greater than 0.5, the cut was considered unstable. Although other methods for determining machining stability have been developed, the stability ratio was applied in this study [15,16]. Fig. 25 also shows the FFT of the audio signal of the milling operations at {4 mm, 6600 rpm} and {4 mm, 9800 rpm}. As seen in Fig. 25, the chatter frequency at 2090 Hz is seen at {4 mm, 6600 rpm} indicating an unstable result. Fig. 26 shows the posterior probability of stability based on the 24 test results using Bayes' learning method described in Section 2. The adaptive experimental strategy using value of information approach was validated using experiments. Before any experimentation, the optimal point was {0.01 mm, 10,600 rpm}.The procedure was as follows:

1 the expected percentage improvement in *MRR* was calculated at each grid point using Eq. (14) and the prior probability of stability;
2 an experiment was performed at the grid point parameters with the highest value of expected percentage improvement in *MRR*;
3 record audio signal during experiment and determine if the test is stable or unstable using the stability ratio;
4 calculate posterior probability of stability; the posterior probability becomes the prior probability for the subsequent update;
5 update the optimal *MRR* if the result is stable;
6 steps 1–5 were repeated till maximum expected percentage improvement in *MRR* is less than 5 %.

As noted, σ_b and σ_{NbT} were 10 % and 3 % of the axial depth of cut and spindle speed range, respectively. Fig. 27 shows the results. From

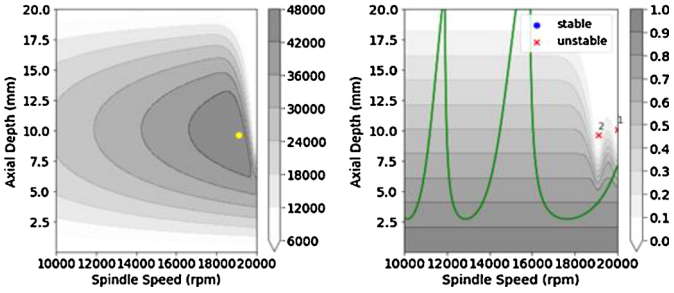

Fig. 20. Expected percentage improvement in *MRR* for the second test (left) and the updated posterior probability after observing an unstable result at the optimal test point.

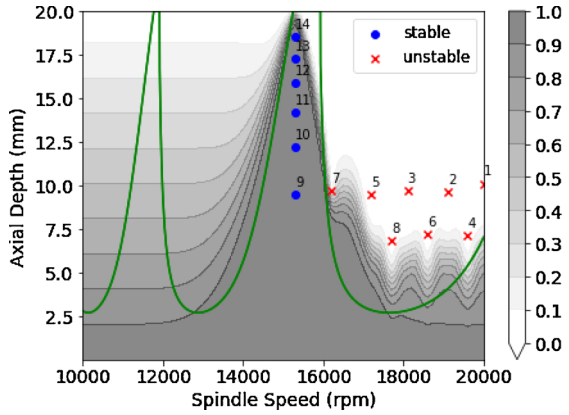

Fig. 21. Test results for optimal parameter identification. The test points are marked based on the order of tests.

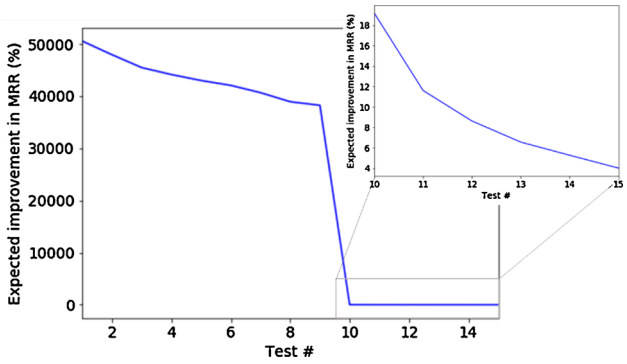

Fig. 22. Maximum expected improvement in *MRR* for each test.

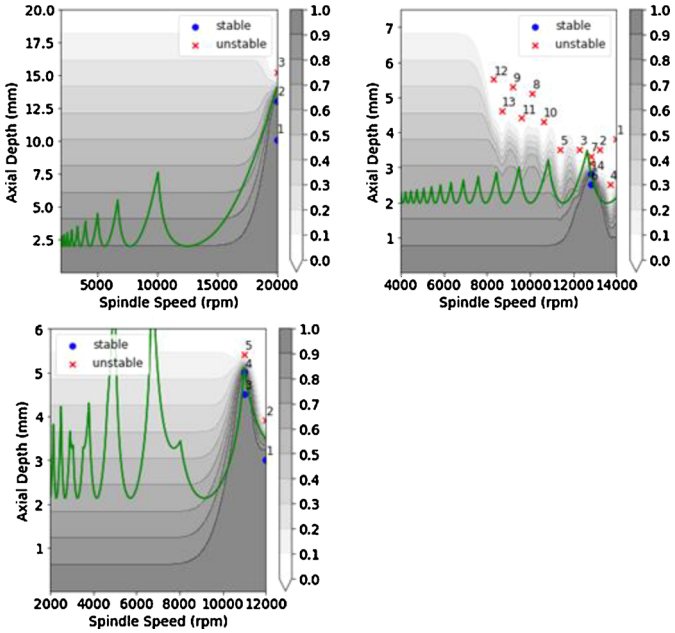

Fig. 23. Experimental search results for Model 2 (top left), Model 3 (top right), and Model 4 (bottom left); results show convergence to the optimal parameters within 3 to 14 tests.

Fig. 27, the optimal parameter was {3.81 mm, 9800 rpm}. To compare the performance of the experimental search, analytical stability lobes were calculated. The tool-material specific cutting force coefficient, K_s, was 650 N/mm^2 [17]. Fig. 28 shows the analytical stability lobes. The stability results from the grid-search are also displayed. As seen in

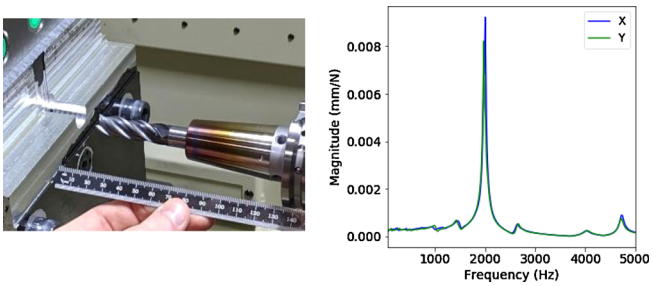

Fig. 24. Experimental setup (left) and tool point frequency response function for the tool (right).

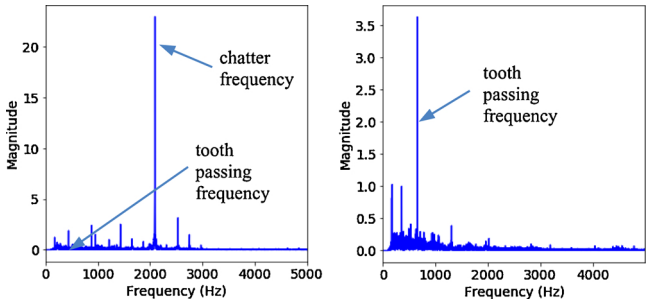

Fig. 25. Spectrum for {4 mm, 6600 rpm} (left) and {4 mm, 9800 rpm} (right); the chatter frequency at 2100 Hz is seen at 6600 rpm indicating chatter.

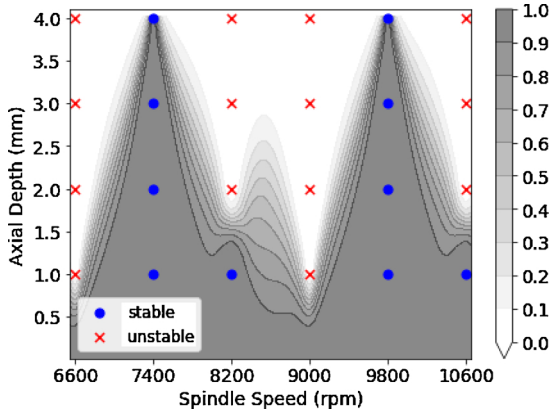

Fig. 26. Posterior probability of stability using 24 experimental results.

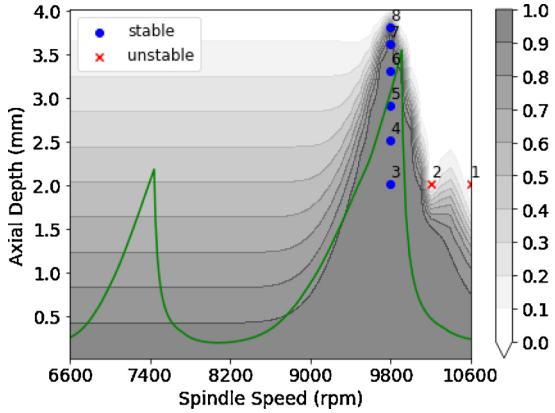

Fig. 27. Experimental results for optimal parameter identification.

Fig. 28, the analytical lobes underpredict the stability limit at 7400 rpm and 9800 rpm. This is due to uncertainty in the frequency response function and the material force coefficients, and assumptions in the

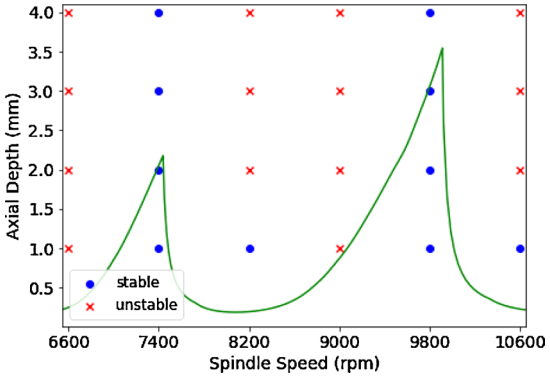

Fig. 28. Analytical stability lobes shown by the solid line along with experimental results from the grid-based approach.

stability model. The Bayes' learning approach identifies a stable point, {3.8 mm, 9800 rpm}, higher than the predicted boundary and converges on the optimal parameters in eight tests without knowledge of the system dynamics or the material cutting force coefficients.

6. Conclusion

A novel Bayesian learning approach for stability lobe and optimal machining parameter identification was presented. The motivation for the approach was to enable learning of the stability boundary when knowledge of the tool point frequency response function and the cutting force coefficients are not known. Results showed that the Bayes' learning method was able to identify the stability boundary with test data. The Bayes' learning method does not require a large number of data points; a single test result updates the probability of stability. This enables continuous learning of the stability boundary in an industrial setting where a large number of data points for every tool-material combination may not be available. An experimental strategy to test at parameters which maximize the maximize the expected percentage improvement in *MRR* was presented. Results showed convergence to the optimal parameters for all stability lobe diagrams within 14 tests with an error of less than 15 %. Future work will focus on utilizing the sensor data during testing to identify the best speeds within the Bayesian framework and developing an experimental strategy to identify the entire stability boundary. In the Bayesian learning methodology described in the paper, knowledge of machining stability was used to guide the learning. Future work will also focus on the application of physics-guided learning to other manufacturing processes.

Acknowledgements

This research was supported by the DOE Office of Energy Efficiency and Renewable Energy (EERE), Energy and Transportation Science Division, and used resources at the Manufacturing Demonstration Facility, a DOE-EERE User Facility at Oak Ridge National Laboratory.

References

[1] Schmitz TL, Smith KS. Machining dynamics: frequency response to improved productivity. Second edition New York, NY: Springer; 2019.
[2] Tlusty J. The stability of the machine tool against self-excited vibration in machining. Proc. Int. Res. in Production Engineering. 1963. p. 465.
[3] Tobias SA, Fishwick W. Theory of regenerative machine tool chatter. Engineer 1958;205(February (7)):199–203.
[4] Merritt HE. Theory of self-excited machine-tool chatter: contribution to machine-tool chatter research. J Inst Eng 1965;87(4):447–54.
[5] Arnold R. Cutting tools research: report of subcommittee on carbide tools: the mechanism of tool vibration in the cutting of steel. Proc Inst Mech Eng 1946;154(Junuary (1)):261–84.
[6] Schmitz TL, Donaldson RR. Predicting high-speed machining dynamics by substructure analysis. CIRP Ann 2000;49(January (1)):303–8.
[7] Budak E, Altintas Y, Armarego EJ. Prediction of milling force coefficients from orthogonal cutting data. 1996. p. 216–24.
[8] Kim HS, Schmitz TL. Bivariate uncertainty analysis for impact testing. Meas Sci Technol 2007;18(October (11)):3565.
[9] Duncan G, Schmitz TL, Kurdi MH. Uncertainty propagation for selected analytical milling stability limit analyses. Trans NAMRI/SME 2000;34:17–24.
[10] Schmitz TL, Duncan GS. Three-point receptance coupling substructure analysis for tool point dynamics prediction. Or tool point dynamics prediction. J Manuf Sci Eng 2005;127(November (4)):781–90.
[11] Karandikar J, Traverso M, Abbas A, Schmitz T. Bayesian inference for milling stability using a random walk approach. J Manuf Sci Eng 2014;136(June (3)):031015.
[12] Karandikar JM, Tyler CT, Abbas A, Schmitz TL. Value of information-based experimental design: application to process damping in milling. Precis Eng 2014;38(October (4)):799–808.
[13] Howard RA. Information value theory. IEEE Trans Syst Sci Cybern 1966;2(August (1)). 22–6.
[14] Howard RA. Decision analysis: perspectives on inference, decision, and experimentation. Proc IEEE 1970;58(May (5)):632–43.
[15] Rubeo MA, Schmitz TL. Amplitude ratio: a new metric for milling stability identification. Procedia Manuf 2017;10(January):351–62.
[16] Schmitz TL. Chatter recognition by a statistical evaluation of the synchronously sampled audio signal. J Sound Vib 2003;262(May (3)):721–30.